FULL PAPER

Rotating-Disk-Based Direct-Current Triboelectric Nanogenerator

Chi Zhang, Tao Zhou, Wei Tang, Changbao Han, Limin Zhang, and Zhong Lin Wang*

An innovative design is reported of a direct-current triboelectric nanogenerator (DC-TENG) based on a rotating disk design for harvesting rotational mechanical energy. The DC-TENG consists of two disks and two pairs of flexible electric brushes that are made of carbon fiber and contact two electrodes, respectively. During the rotation, two disks have distinct triboelectric polarities for a cyclic in-plane charge separation between them and an alternating current is generated between the two electrodes. Because of the sliding contact and automatically switch between the electric brushes and the two electrodes, the current is reversed in the second half of the cycle and a direct current is generated. The role that the rotating speed and the segmentation number have is thoroughly investigated and shows that there is direct current enhancement not only at higher speed but also with more segments. The DC-TENG has been demonstrated as a constant current source for directly and continuously driving electronic devices and/or charging an energy storage unit without a rectifier bridge. This work presents a novel DC-TENG technology and opens up more potential applications for harvesting rotational mechanical energy and powering electronics.

1. Introduction

With the development of micro/nano-electronic devices, power supplying for them has become the focal point of research. Exploratory research for developing self-powered systems that can harvest energy from ambient environment to maintain sustainable operation has attracted increasing interests.[1–5] Mechanical energy widely exists in the natural environment, from which generating electricity is one of the most popular methods for powering electronics based on different effects and mechanisms, such as piezoelectricity,[6–12] electromagnetics,[13,14] and electrostatics.[15,16] Recently, the invention of triboelectric nanogenerators (TENGs) has provided an effective approach to generate electricity by harvesting mechanical energy.[17–23] Based

on the coupling between triboelectrification and electrostatic induction, the periodic mechanical contact and separation between the two surfaces of the TENG with opposite triboelectric charges can drive an alternating flow of electrons between two electrodes through an external load. In previous works, there are mainly two friction modes of the TENG: vertical contact-separation[24,25] and in-plane sliding.[26,27] The output current of the TENG has a much larger peak value but a much shorter pulse in the vertical contact-separation mode, while a much smaller peak value but a longer pulse in the in-plane sliding mode. With the disk or cylindrical rotating TENG,[28,29] there is a continuous and periodic in-plane sliding between the two friction surfaces and the output current has a smoother wave in each half cycle, similar to a sinusoidal function. However, whether the mode is vertical contact-separation or in-plane sliding, the electricity generation process is a periodically repeated cycle, thus the only possible output is alternating-current (AC). Thus a rectifier bridge is required in the back-end processing circuits for regulating the output power for practical use. Because the rectifier bridge is a dissipative unit, and its consumption of power is appreciable if the TENG output is small.

In this work, we developed a direct-current triboelectric nanogenerator (DC-TENG), which consists of two disks and two pairs of flexible electric brushes. This design not only facilitates a rotation-induced periodic, in-plane charge separation for electricity generation, but also introduces a direct current generation method with the flexible electric brushes. This rotating disk and electric brushes based working mechanism was demonstrated. With this DC-TENG, both higher rotating speed and more segments lead to a larger direct-current output. Owing to its direct and continuous current output, multiple light-emitting diodes (LEDs) were lit up directly without a rectifier bridge, and an energy storage unit such as a capacitor was quickly and directly charged. The DC-TENG opens up more important and potential applications of harvesting energy and powering portable electronics.

Dr. C. Zhang, T. Zhou, Dr. W. Tang, Dr. C. Han, L. Zhang, Prof. Z. L. Wang
Beijing Institute of Nanoenergy and Nanosystems
Chinese Academy of Sciences
Beijing 100083, China
E-mail: zlwang@gatech.edu
Prof. Z. L. Wang
School of Material Science and Engineering
Georgia Institute of Technology
Atlanta, GA 30332, USA

2. Results and Discussion

The basic structure of the DC-TENG is composed of two disk-shaped components with one sector of a semi-circle each, as
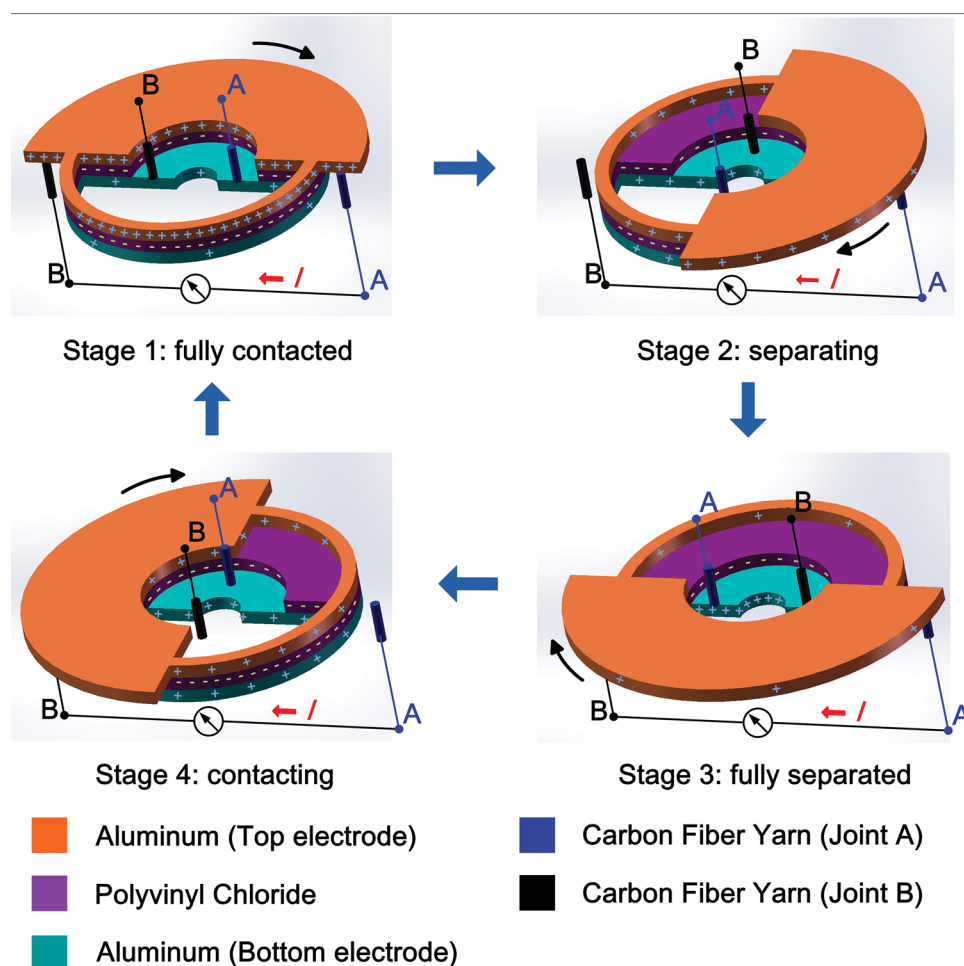
Figure 1. Schematic illustrations showing the proposed working principle of the rotating disk based DC-TENG with the electrons flow diagram in four consecutive stages within a full cycle of direct current output.

schematically illustrated in **Figure 1**. In the fabrication of the disk DC-TENG device, two acrylic sheets were first processed by laser cutting to form the desired semi-circle structured cyclo-style that served as the templates for the effective contacting parts of the DC-TENG. Then, a piece of polyvinyl chloride (PVC) with Al electrode deposited on the back side was manually patterned into the exact shape and then securely attached onto the first sheet. The piece of PVC was tailed into nearly the same shape as the Al electrode but shorter in the center part, so this part of the Al electrode is not covered by the PVC and exposed. Meanwhile, a piece of Al foil was attached onto the second sheet, which was made into nearly the same shape as the piece of PVC but broader in the circular edge part. So when the two pieces of Al foil and PVC were brought to a face-to-face intimate contact, the circular edge part of the Al foil is not contacted with the piece of PVC and exposed. The Al foil was driven to spin clockwise on the surface of the PVC around their common axis. A pair of electric brushes is fixed and located on both outsides of the PVC, respectively, and each of them is alternately contacted with the exposed circular edge part of the Al foil when rotating. While the other pair of electric brushes is located on both insides of the PVC respectively and each of

them is alternately contacted with the exposed center part of the Al electrode when rotating together with the Al foil. The electric brushes are made of carbon fiber and flexible, which can ensure the contact with the electrodes is good and wear-free. One of the fixed electric brushes outside and one of the rotating electric brushes inside have a common joint A, while the other two electric brushes have another common joint B.

The disk DC-TENG in this work presents a different mechanism from the conventional TENG configuration. The working principle of the disk DC-TENG is based on the triboelectrification, the relative-rotation-induced cyclic in-plane charge separation between Al and PVC, and two pairs of flexible electric brushes automatically switch between the two electrodes, as shown in Figure 1. In the relative rotation, the Al surface and PVC surface slide one against the other, so that the electrons will be injected from the Al foil to the surface of the PVC film, leaving net positive charges on the Al foil and net negative charges on the PVC film. The direct current generation process of the disk DC-TENG can be divided into four stages. In stage 1, the two disks are at an overlapping position. Since the rotation is clockwise, the Al foil as the top electrode starts to contact with the electric brush of joint A and separate from the electric brush

www.MaterialsViews.com

ADVANCED
ENERGY
MATERIALS
www.advenergymat.de

FULL PAPER

of joint B. Meanwhile, the Al electrode as the bottom electrode starts to contact with the electric brush of joint B and separate from the electric brush of joint A. As shown in stage 2, when the Al foil rotates in reference to the PVC film, the corresponding two sectors start to have a partially mismatched contact area, which will induce an electron flow from the bottom electrode to the top electrode through an external load, forming a current flow in the direction from joint A to B. In this process, the electrons keep flowing from the bottom electrode to the top electrode until the two disks reach maximal mismatch in the contacting areas, which is represented by stage 3. At this moment, the top electrode starts to contact with the electric brush of joint B and separate from the electric brush of joint A. While the bottom electrode starts to contact with the electric brush of joint A and separate from the electric brush of joint B. In stage 4 as the rotating sheet continues spinning, the PVC surface is contacted with the Al foil again and the overlapping area is increasing. As a result, the electrons will flow back in the opposite direction from the top electrode to the bottom electrode, also forming a current flow in the direction from joint A to B. Thus, the entire process will result in a direct-current (DC) output. Such a charge transfer cycle will start over from stage 1 when the two disks reach a complete overlapping again. **Figure 2**a shows the equivalent circuit diagrams in the first and second half of the cycle.

Obviously, there is still an alternating-current from the top electrode to the bottom electrode during the full cycle. Because of the sliding contact and automatically switch between the electric brushes and the two electrodes, the current is reversed in the second half of the cycle and a direct current in the direction from joint A to B is generated continuously.

As schematically illustrated in Figure 2b, the other various structures of the rotating disk based DC-TENG have been designed and fabricated, in which the two disk-shaped components have two sectors of quarter-circle, three sectors of sixth-circle and four sectors of eighth-circle, respectively. The locations of two pairs of electric brushes are configured according to the different structures, corresponding to the equivalent circuit diagrams in the full cycle as shown in Figure 2a. A photograph of the two parts of a real eighth-circle rotating disk based DC-TENG is shown in Figure 2c. The diameter of two disks is 2.4 inch and the total effective area of the DC-TENG device is 7.91 cm².

As our previous research on the disk TENG, the absolute value of the short-circuit current density (J_{SC}) between the two electrodes is proportional to the disk rotating speed, which can be represented as:[28]

$$|J_{SC}| = \frac{\sigma_0}{\theta_0} \times 2\pi \times \frac{n}{60} \tag{1}$$
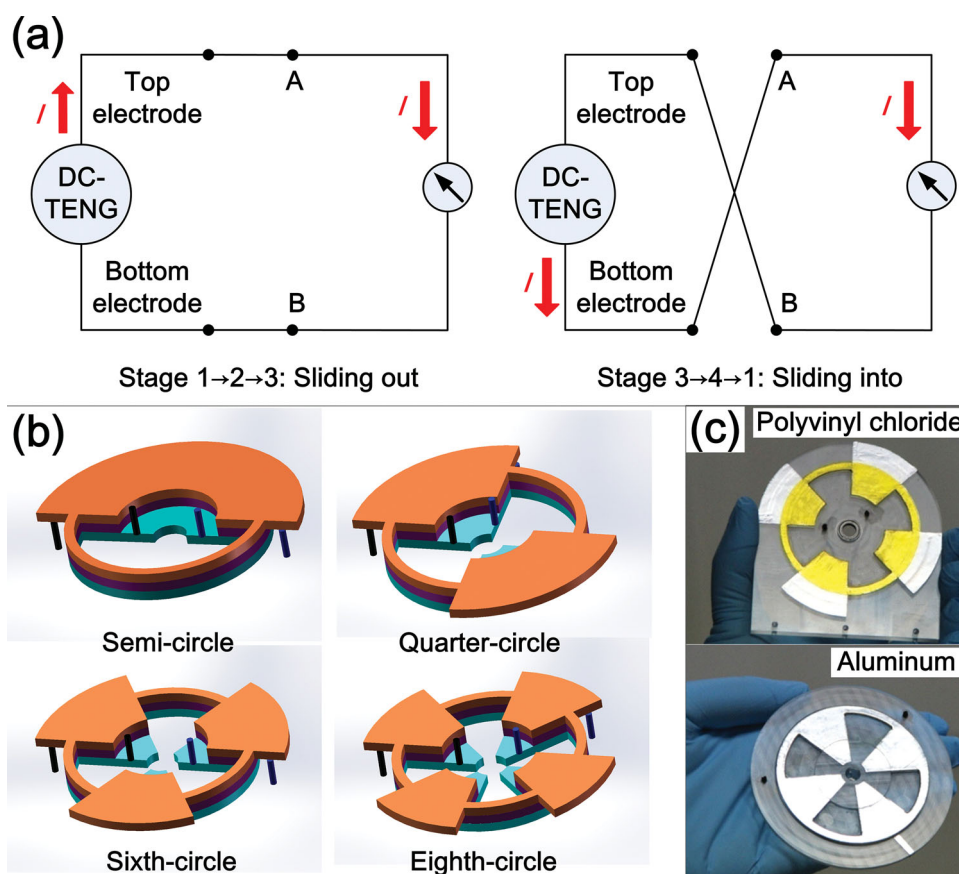

Figure 2. Equivalent circuit diagrams and various structures of the rotating disk based DC-TENG. a) Equivalent circuit diagrams of the rotating disk based DC-TENG showing the connection of the two joints and the two electrodes in different stages. b) Schematic illustrations showing the various structures of the rotating disk based DC-TENG, including the semi-circle, quarter-circle, sixth-circle and eighth-circle. c) A photograph showing the two parts of a real rotating disk based DC-TENG.
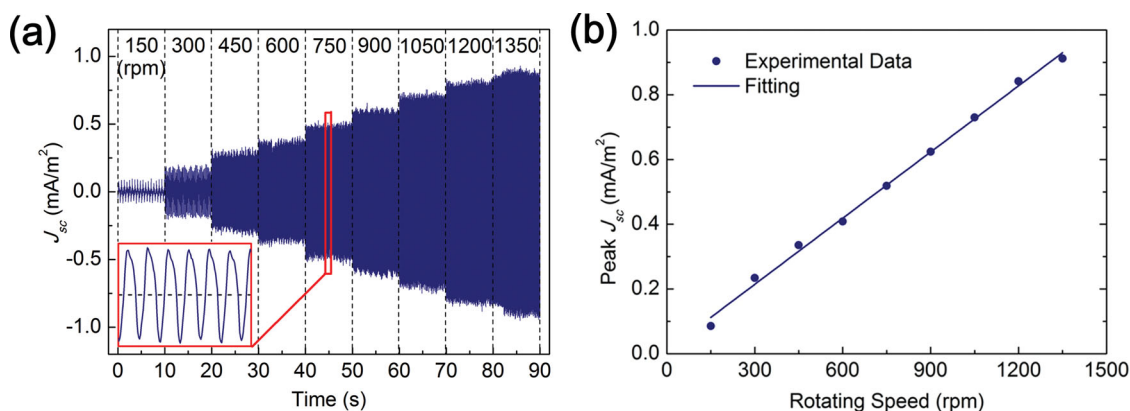
Figure 3. Influence of the rotating speed on the alternating current output performance between the two electrodes of the semi-circle rotating disk based DC-TENG. a) The measured short-circuit current density with different rotating speeds from 150 to 1350 rpm. b) The summarized relationship between the short-circuit current density and the rotating speed.

where σ_0 is a constant value of triboelectric charge density, θ_0 is the disk rotating angle in a half cycle (measured in radian) and n is the disk rotating speed in a unit of rounds per minute (rpm). **Figure 3**a shows the measured short-circuit current density between the two electrodes of the semi-circle DC-TENG with different rotating speeds from 150 to 1350 rpm. An enlarged view in the inset exhibits continuous AC output at 750 rpm. The peak J_{SC} is enhanced with higher rotating speed and the good linear fitting in Figure 3b is coherently consistent to Equation (1). The schematic and circuit diagrams of AC measurement between the two electrodes are illustrated in Figure S1 and S2.

The short-circuit current density between the two joints A and B of the semi-circle DC-TENG is measured as shown in

Figure 4a, with different rotating speeds from 150 to 1350 rpm as well. An enlarged view in the inset exhibits continuous DC output at 750 rpm. The experimental results indicate that the AC between the two electrodes is converted into the DC between the two joints with the electric brushes and verify the aforementioned working principle. A constant DC output can be received when the rotating speed is constant and the DC output has a linear relationship to the rotating speed, which is shown in Figure 4b with approximately the same proportion of the AC output. Figure 4c shows a circuit diagram and a snapshot of directly and continuously powering green LEDs in series by the DC-TENG working at 750 rpm, rather than using indispensable rectifier bridge in previous works.[30] The experimental results indicate that the DC-TENG can be used as
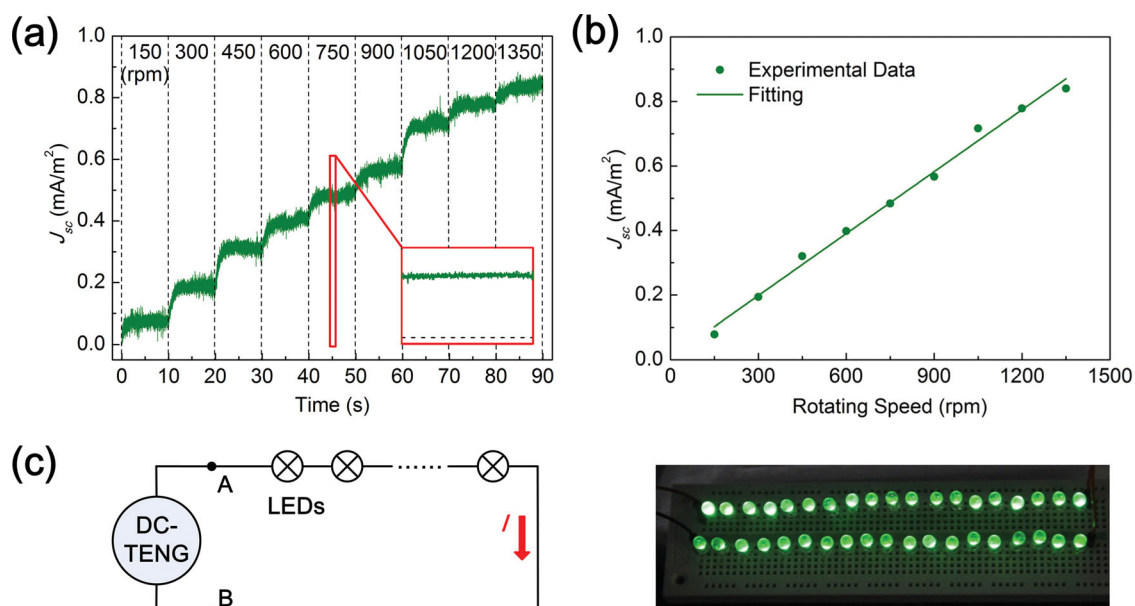

Figure 4. Influence of the rotating speed on the direct current output performance of the semi-circle rotating disk based DC-TENG. a) The measured short-circuit current density with different rotating speeds from 150 to 1350 rpm. b) The summarized relationship between the short-circuit current density and the rotating speed. c) A circuit diagram and a snapshot of directly and continuously powering green LEDs in series without a rectifier bridge by the DC-TENG working at 750 rpm.
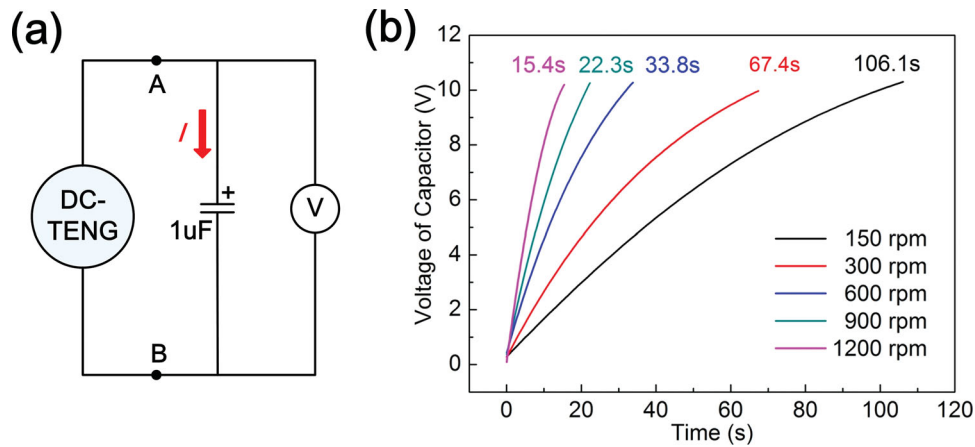
www.MaterialsViews.com

ADVANCED
ENERGY
MATERIALS
www.advenergymat.de

FULL PAPER

Figure 5. Influence of the rotating speed on the charging performance of the quarter-circle rotating disk based DC-TENG. a) A circuit diagram of directly and continuously charging capacitor of 1μF without a rectifier bridge. b) The measured voltage of a 1 μF capacitor charged by the DC-TENG and charging times from 0 V to 10 V at variable rotating speeds.

an efficient power source for directly and continuously driving electronic devices.

Besides, such constant and direct current output imply its capability of directly and continuously charging energy storage units. As shown in **Figure 5**a, a 1μF capacitor was directly charged by the DC-TENG with variable rotating speeds at 150, 300, 600, 900, and 1200 rpm. The capacitor's voltage is measured as shown in Figure 5b, which indicates the capacitor charging rate is increased with higher rotating speed. Compared to the previous charging method with rectifier bridge,[22] the direct charging of an energy storage unit by the DC-TENG will largely improve the practicability of the TENG as a constant current source for electronics.

Figure S3 and S4 show the output current density and voltage of the DC-TENG applied on the resistance of 100 MΩ with different rotating speeds from 150 to 1350 rpm. For different practical applications, the DC-TENG is usually applied on external loads with variable resistances. The output performance of the DC-TENG working at 750 rpm was systematically studied at different loads. **Figure 6**a shows the resistance dependence of both output current density and voltage, from 10 Ω to 5 GΩ. The

output current density decreases with the increasing resistance while the output voltage shows the reverse trend, but both the current and voltage tend to saturate at both high and low ends of the resistance. The power density was also calculated by:

$$P_A = U \cdot J \qquad (2)$$

where P_A is the output power density, U and J are the voltage and the current density on the load with a certain resistance, respectively. The power density was also plotted as a function of external resistance in Figure 6b. The output power density increases at a lower resistance region and then decreases at a higher resistance region. The maximum value of the power density of 25 mW m^{-2} is received at 107 MΩ.

The rate of the triboelectric charge separation relies on not only the disk rotating speed, but also the disk structure. The segments number of the disk is expected to play a significant role in the output performance of the DC-TENG. For this regard, we studied three other types of DC-TENG devices in addition, which have two sectors of quarter-circle, three sectors of sixth-circle and four sectors of eighth-circle, respectively. The
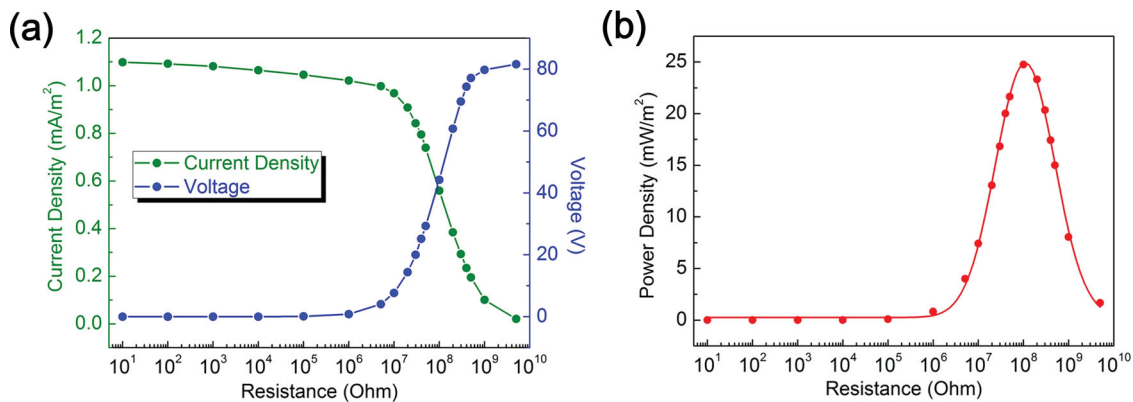

Figure 6. Output performance with different external resistive load of the quarter-circle rotating disk based DC-TENG. a) The relationship between the output voltage/current and the resistance of an external resistive load at 750 rpm. b) The relationship between the effective power density and the resistance of the external load. The maximum power is received when the external resistance is 107 MΩ.
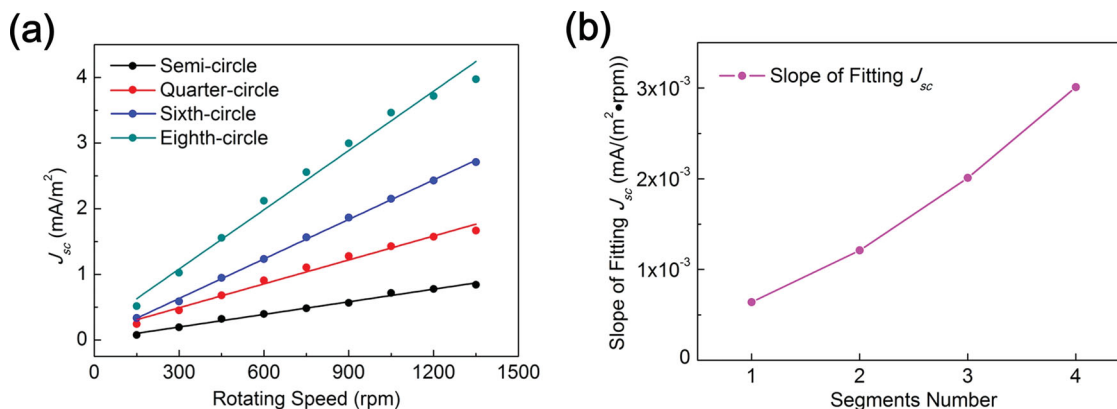
Figure 7. Influence of the segments number on the direct current output performance of the rotating disk based DC-TENG. a) The summarized relationship between the short-circuit current density and the rotating speed of the various structures. b) The summarized relationship between the slopes of the fitting short-circuit current density and the segments number.

direct current output performance is measured to demonstrate the effect of different segments number, as given in **Figure 7**a. An ascending trend of the slope of the fitting J_{SC} with the more segments number is described in Figure 7b, mainly owing to the obvious increasing of the charge transferring rate due to the smaller rotation angle from maximal contact to maximal separation. The experimental results fit well with Equation (1) and the short-circuit direct current output (I_{SC}) of the DC-TENG can be described as the following equation:

$$I_{SC} = \frac{\sigma_0}{\theta_0} \cdot 2\pi \cdot \frac{n}{60} \cdot S = \frac{N}{\pi} \cdot \sigma_0 \cdot S \cdot \omega \tag{3}$$

where S is a constant value of the friction area of the difference between maximal contact and maximal separation, N is the segments number and Ω is angular velocity in a unit of rad/s. Obviously, the direct current output enhancement not only at higher speed but also with more segments. Patterning the disk with much finer segmentations using the techniques of micromachining could greatly improve the output performances and the TENG as a constant current source with large direct current output performance can be highly expected.

3. Conclusion

In summary, we present an innovative design of a direct-current triboelectric nanogenerator based on rotating disk and flexible electric brushes, which can convert rotational mechanical energy into direct-current electricity without using a rectifier bridge. The structure design of the DC-TENG with the electric brushes was described in details to gain a comprehensive understanding about the fundamental working principle, and the experimental results are in good agreement with the design principle and theoretical model. The role played by the rotating speed and the segmentation number was investigated, which shows the direct current enhancement not only at higher speed but also with more segments. By harvesting rotational mechanical energy, the rotating disk based DC-TENG makes it possible to work as a constant current source with large direct current output, showing the great advantages over previous TENG in

directly and continuously driving electronic devices and/or charging an energy storage unit without a rectifier bridge. This work opens up more potential applications for harvesting rotational mechanical energy and powering electronics with DC-TENG as a constant current source.

Supporting Information

Supporting Information is available from the Wiley Online Library or from the author.

Acknowledgements

[1] B. Z. Tian, X. L. Zheng, T. J. Kempa, Y. Fang, N. F. Yu, G. H. Yu, J. L. Huang, C. M. Lieber, *Nature* **2007**, *449*, 885.

[2] M. S. Dresselhaus, G. Chen, M. Y. Tang, R. G. Yang, H. Lee, D. Z. Wang, Z. F. Ren, J. P. Fleurial, P. Gogna, *Adv. Mater.* **2007**, *19*, 1043.

[3] S. Xu, Y. Qin, C. Xu, Y. G. Wei, R. S. Yang, Z. L. Wang, *Nat. Nanotechnol.* **2010**, *5*, 366.

[4] Z. L. Wang, G. Zhu, Y. Yang, S. H. Wang, C. F. Pan, *Mater. Today* **2012**, *15*, 532.

[5] Z. L. Wang, W. Z. Wu, *Angew. Chem., Int. Ed.* **2012**, *51*, 11700.

[6] Z. L. Wang, J. H. Song, *Science* **2006**, *312*, 242.

[7] Y. Qin, X. D. Wang, Z. L. Wang, *Nature* **2008**, *451*, 809.

[8] C. E. Chang, V. H. Tran, J. B. Wang, Y. K. Fuh, L. W. Lin, *Nano Lett.* **2010**, *10*, 726.

[9] X. Chen, S. Y. Xu, N. Yao, Y. Shi, *Nano Lett.* **2010**, *10*, 2133.

[10] Y. F. Hu, L. Lin, Y. Zhang, Z. L. Wang, *Adv. Mater.* **2012**, *24*, 110.

[11] L. Gu, N. Y. Cui, L. Cheng, Q. Xu, S. Bai, M. M. Yuan, W. W. Wu, J. M. Liu, Y. Zhao, F. Ma, Y. Qin, Z. L. Wang, *Nano Lett.* **2013**, *13*, 91.

[12] K. I. Park, C. K. Jeong, J. Ryu, G. T. Hwang, K. J. Lee, *Adv. Energy Mater.* **2013**, *3*, 1539.

[13] C. B. Williams, C. Shearwood, M. A. Harradine, P. H. Mellor, T. S. Birch, R. B. Yates, *Proc. IEEE Circ. Dev. Syst.* **2001**, *148*, 337.

[14] S. P. Beeby, R. N. Torah, M. J. Tudor, P. Glynne-Jones, T. O'Donnell, C. R. Saha, S. Roy, *J. Micromech. Microeng.* **2007**, *17*, 1257.

[15] P. D. Mitcheson, P. Miao, B. H. Stark, E. M. Yeatman, A. S. Holmes, T. C. Green, *Sens. Actuators A* **2004**, *115*, 523.

[16] Y. Naruse, N. Matsubara, K. Mabuchi, M. Izumi, S. Suzuki, *J. Micromech. Microeng.* **2009**, *19*, 094002.

[17] F. R. Fan, Z. Q. Tian, Z. L. Wang, *Nano Energy* **2012**, *1*, 328.

[18] F. R. Fan, L. Lin, G. Zhu, W. Z. Wu, R. Zhang, Z. L. Wang, *Nano Lett.* **2012**, *12*, 3109.

[19] G. Zhu, C. F. Pan, W. X. Guo, C. Y. Chen, Y. S. Zhou, R. M. Yu, Z. L. Wang, *Nano Lett.* **2012**, *12*, 4960.

[20] X. S. Zhang, M. D. Han, R. X. Wang, F. Y. Zhu, Z. H. Li, W. Wang, H. X. Zhang, *Nano Lett.* **2013**, *13*, 1168.

[21] Y. Yang, L. Lin, Y. Zhang, Q. S. Jing, T. C. Hou, Z. L. Wang, *ACS Nano* **2012**, *6*, 10378.

[22] X. Y. Xue, P. Deng, B. He, Y. X. Nie, L. L. Xing, Y. Zhang, Z. L. Wang, *Adv. Energy Mater.* **2013**, DOI: 10.1002/aenm.201301329.

[23] Z. L. Wang, *ACS Nano* **2013**, *7*, 9533.

[24] S. H. Wang, L. Lin, Z. L. Wang, *Nano Lett.* **2012**, *12*, 6339.

[25] G. Zhu, Z. H. Lin, Q. S. Jing, P. Bai, C. F. Pan, Y. Yang, Y. S. Zhou, Z. L. Wang, *Nano Lett.* **2013**, *13*, 847.

[26] S. H. Wang, L. Lin, Y. N. Xie, Q. S. Jing, S. M. Niu, Z. L. Wang, *Nano Lett.* **2013**, *13*, 2226.

[27] G. Zhu, J. Chen, Y. Liu, P. Bai, Y. S. Zhou, Q. S. Jing, C. F. Pan, Z. L. Wang, *Nano Lett.* **2013**, *13*, 2282.

[28] L. Lin, S. H. Wang, Y. N. Xie, Q. S. Jing, S. M. Niu, Y. F. Hu, Z. L. Wang, *Nano Lett.* **2013**, *13*, 2916.

[29] P. Bai, G. Zhu, Y. Liu, J. Chen, Q. S. Jing, W. Q. Yang, J. S. Ma, G. Zhang, Z. L. Wang, *ACS Nano* **2013**, *7*, 6361.

[30] J. W. Zhong, F. R. Fan, Y. Zhang, S. H. Wang, B. Hu, Z. L. Wang, J. Zhou, *Nano Energy* **2013**, *2*, 491.